Range Extension Control System for Electric Vehicle Based on Searching Algorithm of Optimal Front and Rear Driving Force Distribution

Hiroshi Fujimoto and Sho Egami
The University of Tokyo
5-1-5, Kashiwanoha, Kashiwa, Chiba 227-8561 Japan
Email: fujimoto@k.u-tokyo.ac.jp

Jun Saito and Kazunori Handa
MITSUBISHI MOTORS CORPORATION
1, Nakashinkiri, Hashime-cho, Okazaki 444-8501 Japan
Email: kazunori.handa@mitsubishi-motors.com

***Abstract*—Electric vehicles have a disadvantage in that the cruising distance per charge is short. This paper proposes a range extension control system based on a searching algorithm of front and rear driving force distribution with total efficiency optimization. The proposed method maximizes the total efficiency considering the slip ratio and the losses in the motors and inverters. The effectiveness of the proposed method is verified by experiments using a plug-in hybrid electric vehicle. The mileage per charge can be extended by 18% by using the proposed method in a constant-speed test.**

I. Introduction

Nowadays, hybrid vehicles (HVs) and electric vehicles (EVs) are receiving attention because of environmental concerns such as global warming, exhaustion of fossil fuels, and air pollution. In particular, the environmental performance of EVs is superior to that of HVs because their greenhouse gas emissions are zero. In addition, EVs driven by electric motors have four advantages [1], [2]. First, the development of in-wheel motors enables the individual control of each wheel. Second, continuous, smooth braking torque can be generated by regeneration. Third, the generated torque can be measured precisely from the motor current. Finally, quick torque response is available through motor current control. These advantages help us to achieve effective vehicle motion control. Therefore, our research group has studied slip ratio control based on quick torque response and vehicle motion control by using the difference between left and right driving forces [3][4].

EVs have several advantages in terms of environmental performance as well as vehicle motion control. However, the use of EVs leads to several technical problems, preventing their widespread use. Three of the problems that are often encountered are as follows. First, EVs are more expensive than internal combustion engine vehicles. Second, there are very few EV charging facilities. Finally, the cruising distance per charge is very short. In particular, the mileage per charge is insufficient. For solving this problem, several studies have been conducted with the aim of enhancing motor efficiency. A variable-parameter permanent-magnet motor was developed in [5] that can change magnetic flux according to the motor speed. Moreover, a novel drive method for the motor was proposed in [6], wherein the motor is driven with high efficiency using two reduction gears. However, for solving this problem definitively, it is believed that an improvement in battery capacity is necessary.

Our research group has been developing range extension control systems (RECSs) to enhance the cruising range of EVs using control technologies. Here, "range" refers to the cruising range, which is the distance that can be traveled by the vehicle on a single charge. Two types of RECS have already been proposed. The first involves optimizing the efficiency between the electric source and motor output [7]. The second optimizing the efficiency between the motor output and translational speed and yaw rate [8]. We assumed that an EV has more than one motor and that suitable torque distribution results in improved efficiency.

In this paper, an RECS based on front and rear driving force distribution with total efficiency optimization is proposed. The proposed method considers all losses between total input power and total driving force. Conventional vehicle systems distribute the driving force in a fixed distribution ratio to the front and rear wheels. The proposed method optimizes the total efficiency between total input power and total driving force by optimally distributing the driving force among the front and rear wheels. The optimum driving force ratio is determined by a search algorithm using the golden section method [9], [10]. The golden section method is very fast and does not require the vehicle model's derived function. Thus, this search algorithm is not influenced by variations in the parameters of the vehicle, motor, and inverter.

II. Experimental Vehicle and Vehicle Modeling

A. Experimental Vehicle

In this section, our experimental vehicle is described. A plug-in hybrid electric vehicle (PHEV) developed by Mitsubishi Motors Corporation was used in our experiments. This vehicle was equipped with two motors and two differential gears for the front and rear wheels. These motors can be driven independently by two inverters. Figs. 1 and 2 show the PHEV and its electrical system. In Fig. 2, the battery output voltage and the input current to the motor inverters are measurable. These measured variables are used to calculate

Fig. 1. Experimental Vehicle

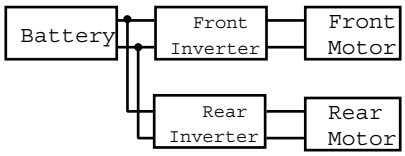

Fig. 2. Vehicle System

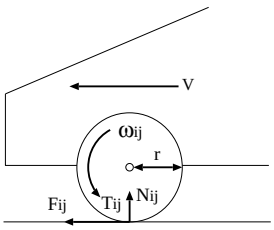

Fig. 3. Wheel Model

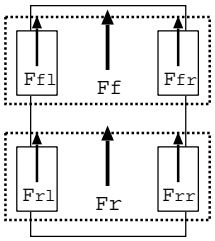

Fig. 4. Driving Force Distribution Model

the total input power. Although this prototype PHEV has an internal combustion engine, we used energy only from the vehicle's battery for evaluating the proposed RECS as battery electric vehicle.

B. Vehicle Modeling

In this section, the vehicle model is explained. From the wheel model and the total driving force model, as shown in Figs. 3 and 4, the equations of wheel- and vehicle motion are as follows:

$$\begin{aligned} J_{w_i}\dot{\omega}_{ij} &= T_{ij} - rF_{ij}, && (1)\\ MV &= F_{ref}, && (2)\\ F_{ref} &= F_{fl} + F_{fr} + F_{rl} + F_{rr}, && (3)\\ V_{w_{ij}} &= r\omega_{ij}, && (4) \end{aligned}$$

where ω_{ij} [rad/s] is the wheel's angular velocity, V [m/s] is the vehicle's velocity, $V_{w_{ij}}$ [m/s] is the wheel's velocity, T_{ij} [Nm] is the wheel torque, F_{ij} [N] is the driving force, M [kg] is the vehicle's mass, r [m] is the radius of the wheel, and J_{wi} [Nms^2] is inertia of the wheel. The subscript i is substituted with f or r, denoting the front or rear wheel, respectively. The subscript j is substituted with l or r, denoting the left or right wheel, respectively.

The slip ratio is defined as follows:

$$\lambda_{ij} = \frac{V_{w_{ij}} - V}{\max(V_{w_{ij}}, V, \epsilon)} \quad (5)$$

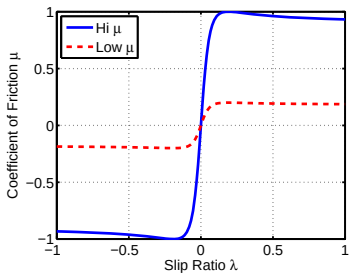

Fig. 5. Typical relationship between μ and λ

where $\epsilon \ll 1$ is a small constant value for avoiding a zero denominator. Generally, $\lambda_{ij} > 0$ when the vehicle is being driven and $\lambda_{ij} < 0$ under braking. Because this paper assumes that the vehicle is being driven, $\lambda_{ij} > 0$ and $\max(V_{w_{ij}}, V, \epsilon) = V_{w_{ij}}$ at all times. sider powering operation only. The slip ratio λ_{ij} is represented by

$$\lambda_{ij} = \frac{V_{w_{ij}} - V}{V_{w_{ij}}}. \quad (6)$$

The friction coefficient μ_{ij} between the tire and the road is a function of the slip ratio λ_{ij}, as shown in Fig. 5. The driving force F_{ij} can be represented as a product of the friction coefficient μ_{ij} and the normal force N_{ij} in the following manner:

$$F_{ij} = \mu_{ij}(\lambda_{ij})N_{ij}. \quad (7)$$

The driving force can be modeled as follows:

$$\begin{aligned} F_{ij} &\simeq D'_s N_{ij}\lambda_{ij}, && (8)\\ D'_s &= \frac{\partial \mu}{\partial \lambda}\,|_{\lambda=0}, && (9) \end{aligned}$$

where D'_s is a coefficient that depends on the road and tire conditions. When the slip ratio λ_{ij} is small, the friction coefficient μ_{ij} is linearly proportional to the slip ratio λ_{ij}. Because only high-friction road tests were performed in this study, the slip ratio can be assumed to be in the linear region $\lambda_{ij} < \lambda_{peak}$. Therefore, the approximation of (8) is valid.

Here, the influence of load transfer caused by longitudinal acceleration is explained. When the vehicle accelerates, the normal force acting on the front and rear wheels is given as follows:

$$\begin{aligned} N_f(a_x) &= \frac{1}{2}\frac{l_r}{l}Mg - a_x M\frac{h_g}{l}, && (10)\\ N_r(a_x) &= \frac{1}{2}\frac{l_f}{l}Mg + a_x M\frac{h_g}{l}, && (11) \end{aligned}$$

where a_x[m/s^2] is the longitudinal acceleration, l_f and l_r are the distance from the center of gravity to front and rear axle tread, respectively, and h_g is the height of the center of gravity.

III. Driving Force Distribution Control

A. Driving Force Distribution Model

In this section, the driving force distribution model is explained. The total driving force of a vehicle is the sum of the driving force at each wheel. Therefore, the driving force

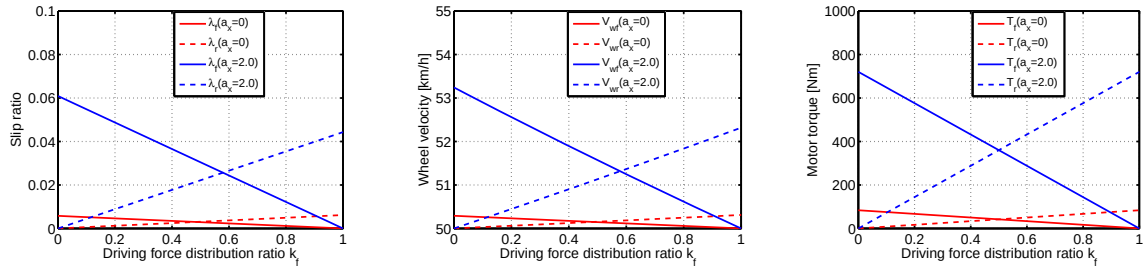

(a) Slip ratio (b) Wheel velocity (c) Wheel torque

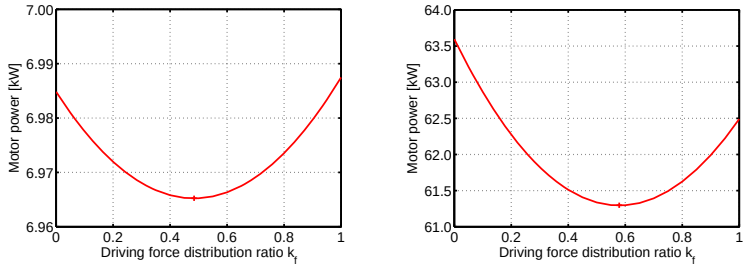

(d) Total motor output ($a_x = 0$) (e) Total motor output ($a_x = 2.0$)

Fig. 6. Simulation of Power Calculation

at each wheel can be set to a different value for achieving the optimal operation point in real time, as long as the total driving force matches the driver's force requirement F_{ref}.

The driving force distribution ratio k_f for the total driving force is introduced. The driving force at each wheel is defined as follows:

$$F_{ref} = F_f + F_r \quad (12)$$
$$F_f = (1 - k_f)F_{ref} \quad (13)$$
$$F_r = k_f F_{ref}, \quad (14)$$

where F_f and F_r are the sums of the left and right wheels, respectively, which are determined as follows:

$$F_f = F_{fl} + F_{fr} \quad (15)$$
$$F_r = F_{rl} + F_{rr}. \quad (16)$$

The driving force distribution ratio k_f is defined as $0 \leq k_f \leq 1$ because we do not consider the regenerative braking operation in this study.

B. Total Motor Output Optimization

In this section, an optimization method is introduced for minimizing the total motor output under a given vehicle velocity by considering the slip ratio and normal force. Here, the optimal distribution-ratio k_f is derived for optimizing the efficiency between the total motor output and total driving force. From (1) and (6), the wheel torque and wheel angular velocity, based on slip ratio, are represented as follows:

$$T_{ij} = rF_{ij} + J_{w_{ij}}\dot{\omega}_{ij}, \quad (17)$$
$$\omega_{ij} = \frac{V}{r}\frac{1}{1-\lambda_{ij}}. \quad (18)$$

The wheel torque given by (17) is balanced by the driving force and the rotational inertial force on the wheel. The rotating inertial force is represented as a function of slip ratio as follows:

$$J_{w_{ij}}\dot{\omega}_{ij} = \frac{J_{w_{ij}}}{r}\left(\frac{a_x}{1-\lambda_{ij}} + \frac{V\dot{\lambda}_{ij}}{(1-\lambda_{ij})^2}\right). \quad (19)$$

In this study, the steady state of the driving force is only considered for evaluating losses. Therefore, the derivative term of the slip ratio $\dot{\lambda}_i$ in (19) is ignored.

The motor output and some quantity related to the motor output for total driving force were calculated. In this simulation, the test vehicle's parameters, summarized in Fig. 1, were used. Two different acceleration conditions were considered, wherein the vehicle maintains a constant velocity of 50 km/h and when it is subject to an acceleration of 2.0 m/s^2. The simulation results are shown in Fig. 6; k_f was considered as a variable parameter. In the case of $a_x = 2.0$ m/s^2, only the time at which a velocity of $V = 50$ km/h was attained is shown.

Fig. 6(a) shows that the slip ratio varies for k_f owing to the influence of normal force on the tire, even under the same total driving force. Fig. 6(b) and Fig. 6(c) show that the wheel torque is dominated by the driving force and the wheel velocity is influenced by the slip ratio. It was confirmed that total motor output attains the minimum value at a specific driving distribution ratio, as shown in Figs. 6(d) and 6(e). This k_f is the optimal ratio for maximizing the efficiency from total motor output to total driving force. It is also shown that this ratio changes according to the load transfer.

Here, the abovementioned optimal ratio is derived from the model. The wheel torque model, which ignores the inertial torque $J_{w_{ij}}\dot{\omega}_{ij}$, is given as follows:

$$T_i = rF_i. \quad (20)$$

When the tire is adhesive with the road and has no wheel-spin, the wheel torque is dominated by the torque based on the driving force. Therefore, this assumption is reasonable. The total motor output is the sum of the motor output at the front and rear wheels. From (8), (13), (14), (18), and (20), the total motor power is given as follows:

$$\begin{aligned} P_{out} &= P_{outf} + P_{outr} \\ &= \omega_f T_f + \omega_r T_r \\ &= F_{ref} V \cdot \left(\frac{1-k_f}{1-\lambda_f} + \frac{k_f}{1-\lambda_r} \right) \quad (21) \\ \lambda_f &= \frac{(1-k_f)F_{ref}}{D'_s N_f} \quad (22) \\ \lambda_r &= \frac{k_f F_{ref}}{D'_s N_r} \quad (23) \end{aligned}$$

The ratio for optimizing the efficiency from total motor output to total driving force is determined by solving the partial differential equation $\frac{\partial P_{out}}{\partial k_f} = 0$. This optimal ratio is represented by the following equation:

$$k_{f_{opt_{ff}}}(a_x) = \frac{l_f}{l_f + l_r} + \frac{2h_g}{(l_f + l_r)g} a_x \quad (24)$$

C. Search Technique

The optimal ratio obtained in section III-B is only for minimizing the motor output and does not consider the efficiencies of both the motors and inverters. In [7], the efficiency maps are assumed to be known according to the motor torque and speed. However, this study does not use those maps, which may vary based on environmental and operating conditions.

In this section, we explain the search technique based on the golden section method. Total efficiency optimization is accomplished using this search technique. Moreover, the optimal ratio derived in section III-B is used in the initial step of this searching algorithm for reducing the search time.

The input powers to the front and rear inverters and total input power are defined as follows:

$$\begin{aligned} P_{inf} &= V_{dc} I_{dcf}, \quad (25) \\ P_{inr} &= V_{dc} I_{dcr}, \quad (26) \\ P_{in} &= P_{inf} + P_{inr}, \quad (27) \end{aligned}$$

where V_{dc}[V] is the inverter input voltage, I_{dcf} and I_{dcr} [A] are the front and rear inverter input currents, respectively. In addition, the efficiencies of the front and rear parts and the total efficiency from total input power to total driving force are defined as follows.

$$\begin{aligned} \eta_f &= \frac{F_f V}{P_{inf}} \quad (28) \\ \eta_r &= \frac{F_r V}{P_{inr}} \quad (29) \\ \eta_{all} &= \frac{F_{ref} V}{P_{in}} \quad (30) \end{aligned}$$

The driving force distribution ratio for achieving total efficiency optimization is decided by the search control. In this study, this technique searches the section $[k_{f_L} \;\; k_{f_H}]$ for the point having maximum total efficiency. The maximum range of the section is as follows.

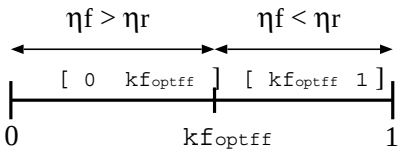

Fig. 7. Initial Section

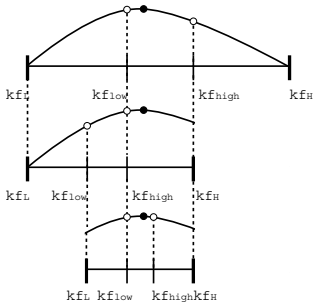

Fig. 8. Concept of search system

- $[k_{f_L} \;\; k_{f_H}] = [0 \;\; 1]$

For reducing the search time, the ratio for minimizing the total motor output, as derived in section III-B, is used here. The initial search section is used for determining the next section to be searched, based on the efficiencies of the front and rear parts. This rule is shown in Fig. 7.

- In case of $\eta_f > \eta_r$
  $[k_{f_L} \;\; k_{f_H}] = [0 \;\; k_{f_{opt_{ff}}}]$
- In case of $\eta_f < \eta_r$
  $[k_{f_L} \;\; k_{f_H}] = [k_{f_{opt_{ff}}} \;\; 1]$

The golden section method is explained here. The searching interval is updated based on the total efficiency at the internally dividing point. The internally dividing point is given as follows:

$$\begin{aligned} k_{f_{low}} &= \alpha k_{f_L} + (1-\alpha) k_{f_H}, \quad (31) \\ k_{f_{high}} &= (1-\alpha) k_{f_L} + \alpha k_{f_H}, \quad (32) \\ \alpha &= \frac{\sqrt{5}-1}{2}, \quad (33) \end{aligned}$$

where α is the golden ratio.

The total efficiency is calculated in each search step T_{step}. If $\eta_{all}(k_{f_{low}}) > \eta_{all}(k_{f_{high}})$, the next section to be searched is $[k_{f_L} \;\; k_{f_{high}}]$. As shown in Fig. 8, the internally dividing point in the new section is updated as follows:

$$\begin{aligned} k_{f_L}[i+1] &= k_{f_L}[i] \quad (34) \\ k_{f_H}[i+1] &= k_{f_{high}}[i] \quad (35) \\ k_{f_{low}}[i+1] &= \alpha k_{f_L}[i+1] + (1-\alpha) k_{f_H}[i+1] \quad (36) \\ k_{f_{high}}[i+1] &= k_{f_{low}}[i] \quad (37) \end{aligned}$$

If $\eta_{all}(k_{f_{low}}) < \eta_{all}(k_{f_{high}})$, the new section to be searched is $[k_{f_{low}} \;\; k_{f_H}]$. Similarly, the internally dividing point in the new section is updated as follows:

$$\begin{aligned} k_{f_L}[i+1] &= k_{f_{low}}[i] \quad (38) \\ k_{f_H}[i+1] &= k_{f_H}[i] \quad (39) \\ k_{f_{low}}[i+1] &= k_{f_{high}}[i] \quad (40) \\ k_{f_{high}}[i+1] &= (1-\alpha) k_{f_L}[i+1] + \alpha k_{f_H}[i+1] \quad (41) \end{aligned}$$

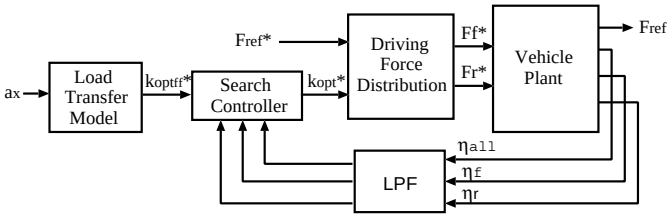

Fig. 9. Proposed Control System

The section to be searched is narrowed by repeating this process. When the section is within a desirable range $k_{f_{high}} - k_{f_{low}} < \epsilon$, the optimum driving force ratio is determined as follows:

$$k_{f_{opt}} = \frac{1}{2}(k_{f_{low}[i]} + k_{f_{high}[i]}) \tag{42}$$

The proposed search control system is shown in Fig. 9. In this study, the driving force commands for front and rear wheels are given as the torque command because a high-friction road and constant velocity motion are assumed.

$$T_i^* = rF_i^* \tag{43}$$

IV. Experiment

To confirm the effectiveness of the proposed RECS, experiments are carried out on a normal asphalt road. To show the convergence speed of this searching algorithm, two conditions of the initial section are compared. One is $[k_{f_L} \quad k_{f_H}]$ = [0 1] for searching the entire range, which is referred to as "Proposal 1." The other is to use the ratio for minimizing the total motor output derived in section III-B, as shown in Fig. 7, and is referred to as "Proposal 2."

The experiment is performed under a constant vehicle speed of 50 km/h. The vehicle speed controller is implemented as the outer-loop PI control of Fig. 9, which corresponds to the driver's model. The vehicle speed V is estimated from the wheel speeds and acceleration.

The PI controller is designed to set the closed-loop poles at $w_n = -1.5$ rad/s for the following nominal model.

$$V = \frac{1}{Ms}F_{ref} \tag{44}$$

This total driving force command is distributed according to the ratio k_f. The measured noise of the feedback signals of η_f, η_r, and η_{all} is attenuated by the following low-pass filter.

$$G(s) = \frac{1}{(0.3s+1)^2} \tag{45}$$

The parameters in the searching algorithm are selected as T_{step} =1.5 s and ϵ =0.05. Fig. 10 shows the experimental results. Except for Fig. 10(c), only the results of "proposal 2" are shown. As shown in Fig. 10(a), Fig. 10(b), and Fig. 10(c), the vehicle settles to a steady speed at around $t = 13$ s, and the searching algorithm is started from $t_0 = 20$ s. From Fig. 10(d) and Fig. 10(e), the total efficiency is improved by around 5.0% and the total input power is reduced by around 1.0 kW at the same vehicle speed by using the searching algorithm.

In Fig. 10(c), "proposal 2" adopts $k_{f_{opt_{ff}}}$ to minimize the total motor output and "proposal 1" adopts the equal distribution ($k_f = 0.5$) before the searching algorithm starts at t_0. In proposal 2, because $\eta_f > \eta_r$, before the search starts at t_0, a limited section, $[k_{f_L} \quad k_{f_H}] = [k_{f_{opt_{ff}}} \quad 1]$, is searched to reduce the searching time. The distribution ratio quickly converges to $k_f \simeq 0.9$ in four steps. However, the ratio converges to $k_f \simeq 0.8$ in six steps when using proposal 1. The reason behind this difference is the variation in the rolling friction, driving resistance, and efficiencies of motors and inverters. Proposal 2 can shorten the convergence time by 3 s (two steps) because the initial section is limited.

To confirm the repeatability, proposed methods 1 and 2 were experimentally examined 12 times. The averaged results of distribution ratio, energy consumption, and improvement in total efficiency are shown in Fig. 11, Fig. 12, and Fig. 13, respectively. The error bar denotes the standard deviation $\pm\sigma$ over 12 measurements. Because the average distribution in proposal 1 ($\bar{k}_f = 0.85$) shows good agreement with that in the proposal 2 ($\bar{k}_f = 0.81$), the validity of the optimization method is confirmed.

In Fig. 12, the conventional method implies equal distribution ($k_f = 0.5$). The average energy consumption is calculated using the total input power for 5 s in the steady state. Even with the same vehicle speed at 50 km/h, a 1.0 kW decrease in energy consumption is achieved using the proposed optimization method. Fig. 13 shows the difference between the total efficiency calculated using the conventional method ($k_f = 0.5$) and that calculated using the proposed method, under steady-state conditions. Both proposed methods 1 and 2 improved the total efficiency by around 5%.

Table I shows the cruising distance per kWh of battery capacity, calculated from Fig. 12. The proposed method extended the cruising range by around 1.52 km/kWh, which corresponds to an 18% increase in distance for the same battery capacity. If this prototype EV has the same battery capacity as the i-MiEV (16 kWh), the cruising range is extended by around 24.2 km using the proposed methods.

TABLE I
Cruising range (km/kWh)

Battery Capacity	Without RECS	With RECS
1 kWh	8.27 km	9.79 km
16 kWh	132.38 km	156.61 km

V. Conclusion

In this paper, a range extension control system was proposed for electric vehicles with front and rear independent motors, based on a searching algorithm for determining the optimal distribution ratio. From the constant-speed experiments performed at a vehicle speed of 50 km/h, this method extended the cruising distance by 18% compared with the conventional equal distribution method.

Future work involves the extension of the proposed searching algorithm to a speed pattern comprising frequent acceler-

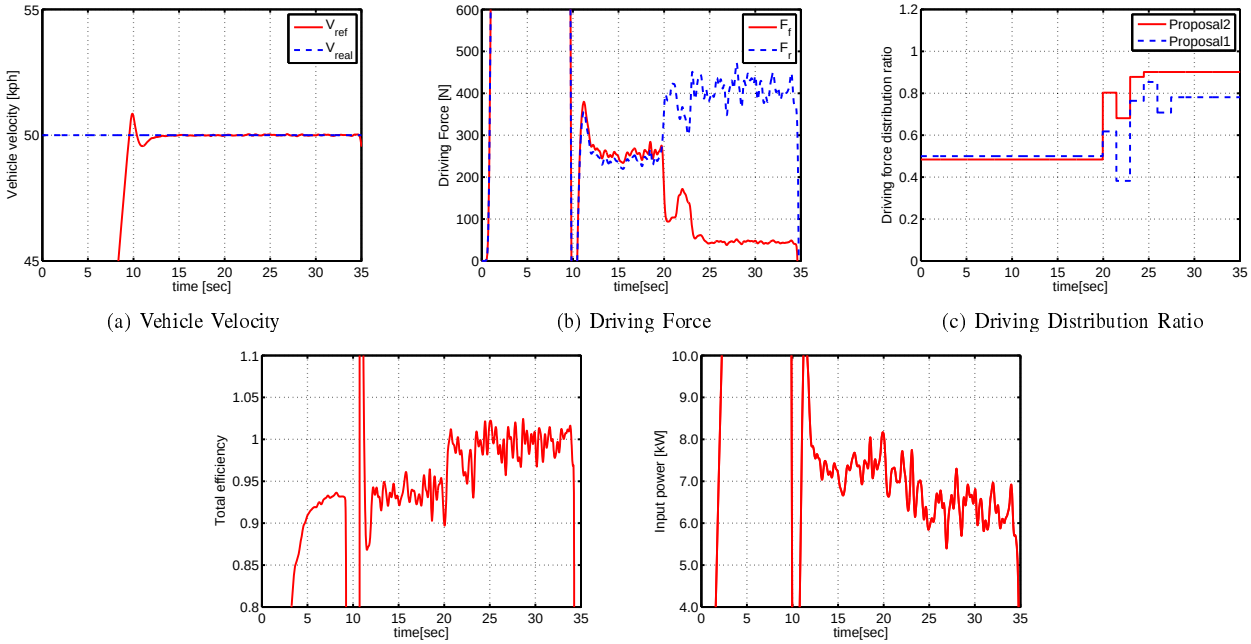

(a) Vehicle Velocity (b) Driving Force (c) Driving Distribution Ratio

(d) Normalized total Efficiency (e) Total Input Power

Fig. 10. Experimental Result

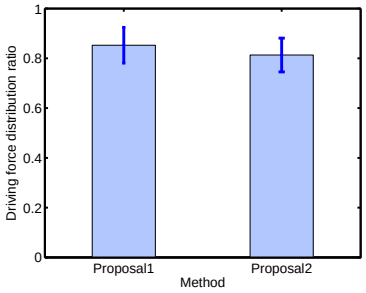

Fig. 11. Final Driving Distribution Ratio

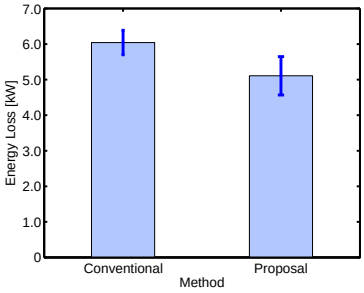

Fig. 12. Average Energy Consumption

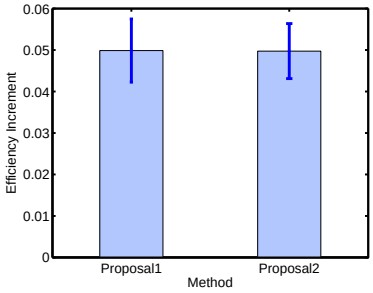

Fig. 13. Increment in Total Efficiency

ation and deceleration and validation of this method using a realistic test pattern such as the JC08 mode.

ACKNOWLEDGMENT

This research was partly supported by the Ministry of Education, Culture, Sports, Science and Technology (Grant number 22246057).

REFERENCES

[1] Y. Hori, "Future vehicle driven by electricity and control – research on four-wheel-motored "UOT electric march II," *IEEE Trans. Industrial Electronics*, vol. 51, no. 5, pp. 954–962, 2004.

[2] M. Kamachi, H. Miyamoto, and H. Yoshida, "Development of electric vehicle for on-road test," in *Proc. 8th International Symposium on Advanced Vehicle Control*, pp. 665–669, 2008.

[3] T. Suzuki and H. Fujimoto, "Slip ratio estimation and regenerative brake control without detection of vehicle velocity and acceleration for electric vehicle at urgent brake-turning," in *The 11th IEEE International Workshop on Advanced Motion Control Proceedings*, pp. 273–278, 2010.

[4] H. Fujimoto and Y. Yamauchi, "Advanced motion control of electric vehicle based on lateral force observer with active steering," in *IEEE International Symposium on Industrial Electronics 2010 Proceedings*, pp. 3627–3632, 2010.

[5] K. Sakai, K. Yuki, Y. Hashiba, N. Takahashi, and K. Yasui, "Principle of the variable-magnetic-force memory motor," in *Proc. International Conference of Electrical Machines and Systems*, pp. 1–6, 2009.

[6] A. Sorniotti, M. Boscolo, A. Turner, and C. Cavallino, "Optimization of a 2-speed gear box for an electric vehicle," in *Proc. 10th International Symposium on Advanced Vehicle Control*, pp. 755–760, 2010.

[7] H. Fujimoto and H. Sumiya, "Range Extension Control System of Electric Vehicle Based on Optimal Torque Distribution and Cornering Resistance Minimization," in *Proc. The 37th Annual Conference of the IEEE Industrial Electronics Society*, pp. 3727–3732, 2011.

[8] H. Sumiya and H. Fujimoto, "Range extension control system for electric vehicle with active front steering and driving/braking force distribution on curving road," in *Proc. The 36th Annual Conference of the IEEE Industrial Electronics Society*, pp. 2823–2828, 2010.

[9] C. -M. Ta, Y. Hori: "Convergence improvement of efficiency-optimized control of induction motor drives," *IEEE Trans. Industry Applications*, Vol. 37, No. 6, pp. 1746–1753, 2001

[10] C. Chakraborty, Y. Hori: "Fast efficiency optimization techniques for the indirect vector-controlled induction motor drives," *IEEE Trans. on Industry Applications*, Vol. 39, No. 4, pp.1070–1076, 2003